

# NAVAL POSTGRADUATE SCHOOL Monterey, California



## THESIS

ANALYSIS OF TURBULENCE MODELS IN A CROSS  
FLOW PIN FIN MICRO-HEAT EXCHANGER

by

Eric K. Lind

June 2002

Thesis Advisor:

Ashok Gopinath

Approved for public release; distribution is unlimited.

THIS PAGE INTENTIONALLY LEFT BLANK

REPORT DOCUMENTATION PAGE			Form Approved OMB No. 0704-0188	
Public reporting burden for this collection of information is estimated to average 1 hour per response, including the time for reviewing instruction, searching existing data sources, gathering and maintaining the data needed, and completing and reviewing the collection of information. Send comments regarding this burden estimate or any other aspect of this collection of information, including suggestions for reducing this burden, to Washington headquarters Services, Directorate for Information Operations and Reports, 1215 Jefferson Davis Highway, Suite 1204, Arlington, VA 22202-4302, and to the Office of Management and Budget, Paperwork Reduction Project (0704-0188) Washington DC 20503.				
1. AGENCY USE ONLY (Leave blank)		2. REPORT DATE June 2002		3. REPORT TYPE AND DATES COVERED Master's Thesis
4. TITLE AND SUBTITLE Analysis of Turbulence Models in a Cross Flow Pin Fin Micro-Heat Exchanger			5. FUNDING NUMBERS	
6. AUTHOR (S) Eric K. Lind				
7. PERFORMING ORGANIZATION NAME(S) AND ADDRESS(ES) Naval Postgraduate School Monterey, CA 93943-5000			8. PERFORMING ORGANIZATION REPORT NUMBER	
9. SPONSORING / MONITORING AGENCY NAME(S) AND ADDRESS(ES)			10. SPONSORING/MONITORING AGENCY REPORT NUMBER	
11. SUPPLEMENTARY NOTES The views expressed in this thesis are those of the author and do not reflect the official policy or position of the U.S. Department of Defense or the U.S. Government.				
12a. DISTRIBUTION / AVAILABILITY STATEMENT Approved for public release; distribution is unlimited.			12b. DISTRIBUTION CODE	
13. ABSTRACT (maximum 200 words)  In this study, several turbulence models are analyzed in a 3-D finite element model of a micro-heat exchanger. The micro-heat exchanger consists of a narrow planar flow passage between parallel walls with small cylindrical pin fins spanning these walls with axes perpendicular to the direction of flow. Turbulence model performance is compared with baseline experimental data available in the literature that cover a range of low turbulent Reynolds numbers and spacing configurations. The metric for these comparisons is an array averaged Nusselt Number. Adjustments made to the coefficients in the turbulence models are explained in terms of their physical significance to the complex flow environment of a pin fin, cross flow, micro-heat exchanger. Applications of this research include cooling of turbine blades and of closely spaced electronics.				
14. SUBJECT TERMS Pin-Fin Array, Compact Heat Exchanger, Heat Transfer, Micro Heat Exchanger, Turbine Blade Cooling			15. NUMBER OF PAGES 59	
			16. PRICE CODE	
17. SECURITY CLASSIFICATION OF REPORT Unclassified	18. SECURITY CLASSIFICATION OF THIS PAGE Unclassified	19. SECURITY CLASSIFICATION OF ABSTRACT Unclassified	20. LIMITATION OF ABSTRACT UL	

NSN 7540-01-280-5500

Standard Form 298 (Rev. 2-89)  
Prescribed by ANSI Std. Z39-18

THIS PAGE INTENTIONALLY LEFT BLANK

Approved for public release; distribution is unlimited.

ANALYSIS OF TURBULENCE MODELS IN A CROSS FLOW PIN FIN  
MICRO-HEAT EXCHANGER

Eric K. Lind  
Lieutenant, United States Navy  
B.S., University of South Carolina, 1995

Submitted in partial fulfillment of the  
requirements for the degree of

MASTER OF SCIENCE IN MECHANICAL ENGINEERING

from the

NAVAL POSTGRADUATE SCHOOL  
June 2002

Author: Eric K. Lind

Approved by: Ashok Gopinath  
Thesis Advisor

Terry McNelley  
Chairman, Department of Mechanical  
Engineering

THIS PAGE INTENTIONALLY LEFT BLANK

## **ABSTRACT**

In this study, several turbulence models are analyzed in a 3-D finite element model of a micro-heat exchanger. The micro-heat exchanger consists of a narrow planar flow passage between parallel walls with small cylindrical pin fins spanning these walls with axes perpendicular to the direction of flow. Turbulence model performance is compared with baseline experimental data available in the literature that cover a range of low turbulent Reynolds numbers and spacing configurations. The metric for these comparisons is an array averaged Nusselt Number. Adjustments made to the coefficients in the turbulence models are explained in terms of their physical significance to the complex flow environment of a pin fin, cross flow, micro-heat exchanger. Applications of this research include cooling of turbine blades and of closely spaced electronics.

THIS PAGE INTENTIONALLY LEFT BLANK

## TABLE OF CONTENTS

I. INTRODUCTION.....	1
II. BACKGROUND AND OBJECTIVES .....	3
A. HEAT EXCHANGER CONSTRUCTION .....	3
B. PREVIOUS WORK.....	4
C. OBJECTIVE.....	5
III. TURBULENCE MODELS.....	7
A. INITIAL MODELING.....	7
1. Boundary Conditions .....	7
2. Initial Conditions .....	9
3. Mesh Structure .....	9
B. SKE MODEL.....	11
C. RENORMALIZED GROUP (RNG) MODEL - DIFFERENCES FROM SKE 17	
D. NKE - DIFFERENCES FROM SKE .....	19
E. FAILURES - ZEM, GIR, SZL .....	21
F. ADVECTION SOLVERS .....	22
IV. RESULTS AND DISCUSSION.....	23
A. NUMERICAL EXPERIMENTS CONDUCTED.....	23
B. TURBULENCE MODEL PERFORMANCE .....	23
1. The SKE Model.....	24
2. The RNG Model.....	28
3. The NKE Model.....	33
V. CONCLUSIONS AND RECOMENDATIONS .....	35
A. OPTIMIZATION OF THE SHORT PIN FIN HEAT EXCHANGER .	35
B. FUTURE PLANS .....	36
LIST OF REFERENCES.....	39
INITIAL DISTRIBUTION LIST .....	41

THIS PAGE INTENTIONALLY LEFT BLANK

## LIST OF FIGURES

Figure 1. Definition sketch of a staggered pin-fin array .....	3
Figure 2. Modeled Portion of a Pin Fin Heat Exchanger .....	8
Figure 3. Actual model used for experiment.....	8
Figure 4. Standard Mesh showing nodes concentrated in the areas of the no slip boundary.....	10
Figure 5. Standard Mesh (Top View) with nodes concentrated around the high velocity regions of the pins .....	10
Figure 6. Changes in the turbulent kinetic energy in the simulated flow field due to a $C_{le}$ increase of 30% at Re=3980.....	26
Figure 7. Change in the turbulent kinetic energy distribution of an RNG run at Re=3980 where $h_{\infty}$ was decreased by 60% .....	31
Figure 8. Change in the temperature distribution of an RNG run at Re=3980 where $h_{\infty}$ was decreased by 60% .....	32

THIS PAGE INTENTIONALLY LEFT BLANK

## LIST OF TABLES

Table 1.	Constants for SKE Model .....	14
Table 2.	RNG Model Coefficients .....	18
Table 3.	NKE Model Coefficients .....	21
Table 4.	Summary of SKE performance when $C_{le}$ is varied.....	25
Table 5.	Summary of SKE performance when $C_2$ , $s_e$ , and $s_k$ are decreased by 30% .....	28
Table 6.	Summary of RNG Performance When $h_\infty$ is Varied.....	29
Table 7.	Summary of NKE Performance .....	34
Table 8.	Optimal Constants for the Cross Flow Pin Fin Heat Exchanger.....	35
Table 9.	Optimal Constants Compared with Metzger's Experimental Values .....	36

THIS PAGE INTENTIONALLY LEFT BLANK

## NOMENCLATURE

$A$	wetted area [ $\text{m}^2$ ]
$C$	turbulence model coefficient
$C_p$	specific heat [ $\text{J/kgK}$ ]
$D$	pin-fin diameter [ $\text{m}$ ]
$E$	law of the wall constant
$g_x$	body acceleration in x direction [ $\text{m/s}^2$ ]
$h$	convection coefficient [ $\text{W/m}^2\text{K}$ ]
$H$	pin height [ $\text{m}$ ]
$K$	thermal conductivity [ $\text{W/mK}$ ]
$k$	turbulent kinetic energy [ $\text{m}^2/\text{s}^2$ ]
LMTD	log mean temperature difference
$\dot{m}$	mass flow rate [ $\text{kg/s}$ ]
$Nu$	Nusselt number
$Re$	Reynolds number
$S$	spanwise spacing between pin centers [ $\text{m}$ ]
$T$	temperature [ $\text{K}$ ]
$T_B$	bulk temperature [ $\text{K}$ ]
$T_{in}$	inlet bulk temperature [ $\text{K}$ ]
$T_{out}$	outlet bulk temperature [ $\text{K}$ ]
$T_S$	surface temperature [ $\text{K}$ ]
$T_W$	wall/pin temperature [ $\text{K}$ ]
$T_8$	free steam temperature [ $\text{K}$ ]
$u'_i$	fluctuating velocity in the i direction [ $\text{m/s}$ ]
$V_{MAX}$	maximum velocity [ $\text{m/s}$ ]
$V_{tan}$	velocity tangent to the wall
$V'_x$	fluctuating velocity in x direction [ $\text{m/s}$ ]
$X$	streamwise spacing between pin centers [ $\text{m}$ ]
$\beta$	bulk modulus
$d$	distance from the wall [ $\text{m}$ ]
$\epsilon$	turbulent kinetic energy dissipation rate [ $\text{m}^2/\text{s}^3$ ]
$\eta$	deformation tensor invariant
$\eta^\infty$	RNG turbulence constant
$\kappa$	slope of the wall parameter
$F$	viscous dissipation term
$\rho$	density [ $\text{kg/m}^3$ ]
$s_t$	turbulent Prandtl number
$s_x^R$	x component Reynolds stress
$\tau$	shear stress [ $\text{kg/ms}$ ]
$\mu_l$	laminar absolute viscosity [ $\text{kg/m s}$ ]
$\mu_t$	turbulent viscosity [ $\text{kg/m s}$ ]
$\mu_w$	wall element effective viscosity [ $\text{kg/m s}$ ]

THIS PAGE INTENTIONALLY LEFT BLANK

## **ACKNOWLEDGEMENTS**

I would like to thank Professor Ashok Gopinath for his undying patience when it comes to teaching the finer points of heat transfer. I would also like to thank Commander Len Hamilton for always seeming to have a grip on the entire project and when all was lost, knowing how to recover some useful data. I appreciate my wife Rachel's patience, understanding and love when I needed to go back into school many nights. You really are the best thing to happen to me. I would especially like to thank my son Daniel. A smile from him let's me know exactly what's important in life.

THIS PAGE INTENTIONALLY LEFT BLANK

## I. INTRODUCTION

High temperatures on power turbine blades have been a limiting factor in advancing the design of gas turbine engines. Conventional cooling schemes in advanced gas turbine engines will be unable to remove the heat transferred from the mass stream fast enough to prevent damage to the blades. A new cooling scheme has been proposed which may be adaptable to the turbine blade cooling problem. It consists of a narrow flow passage between two endwalls is separated by rows of short pin fins with axes perpendicular to the coolant flow. It is envisioned that this flow passage would be tightly "wrapped" around a turbine blade forming a protective cooling shroud. Bleed-off air for cooling would be supplied through the blade root and distributed at the leading edge of the passage flow with an exit to the turbine flow at the trailing edge of the blade. This paper addresses the turbulence models used in the 3-D numerical modeling of two arrangements of this cooling scheme over several low, but fully turbulent Reynolds numbers. The turbulence models have been fine tuned to agree with available experimental data in the literature, and optimal models and coefficients have been identified.

THIS PAGE INTENTIONALLY LEFT BLANK

## II. BACKGROUND AND OBJECTIVES

### A. HEAT EXCHANGER CONSTRUCTION

The micro-heat exchanger modeled in this study is made up of a narrow flow passage supported by 10 staggered rows of pin fins perpendicular to the flow. Figure 1 is a definition sketch of a typical configuration, similar to the type constructed by Metzger, et al. (1982) which forms the basis of corroboration for the current numerical study.

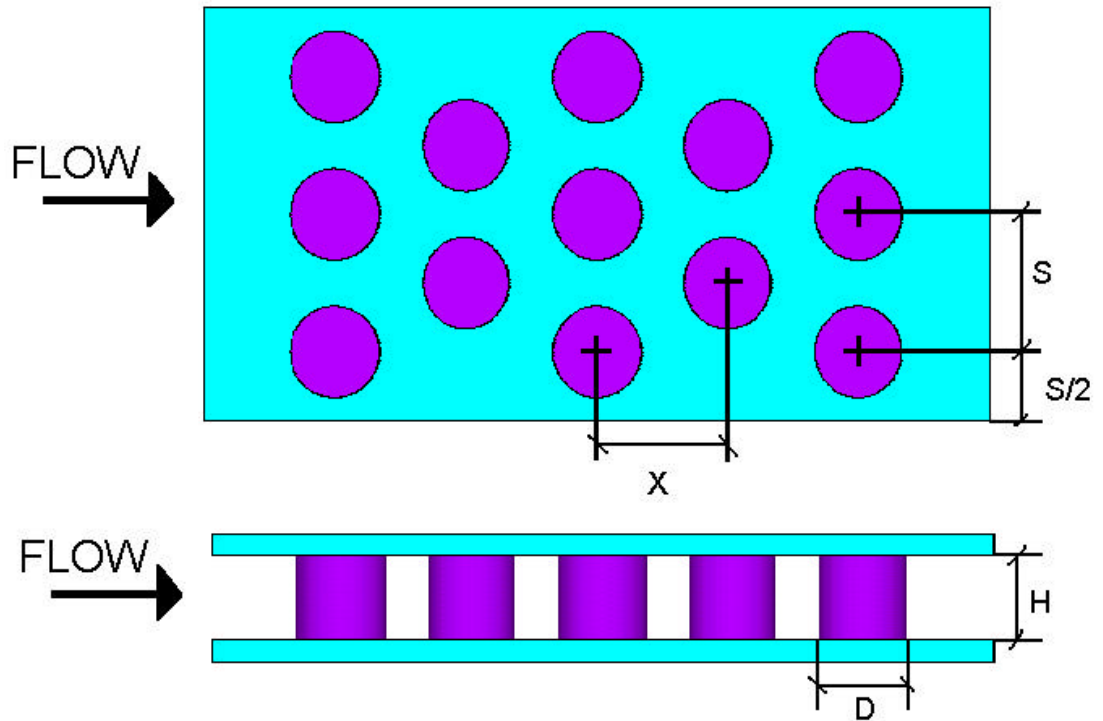


Figure 1. Definition sketch of a staggered pin-fin array

The pins are arranged with a constant axial pitch ( $X$ , distance between pin centers in the flow direction) to form the reference length scale. The axial pitch was chosen to be 12.7mm to be consistent with earlier studies. Two different diameter pins were used in this setup, 8.46mm and

5.08mm. The  $X/D$  and  $S/D$  ratios define the relative streamwise and spanwise pin spacing respectively for a general model. As a result of these settings the transverse pitch ( $S$ ) was not a constant from model to model, although axial pitch was.

As in the work of Metzger et al (1982), the endwalls (the broad upper and lower plates) were modeled as isothermal surfaces. The pins were modeled as isothermal at the temperature of the bounding endwalls as a first approximation. It can be shown with a standard pin fin relation (Incropera and Dewitt, 1996) that the isothermal assumption for the pins is a valid assumption. The side walls were modeled as insulated, again to duplicate Metzger's work and an insulated inlet and outlet section were added (not shown in Figure 1).

## **B. PREVIOUS WORK**

The staggered pin-fin array geometry, in one form or other, serves as the basis for a large number of compact heat exchanger configurations, and has received considerable attention in the past. The experimental work of VanFossen (1982), Metzger et al (1982), Chyu (1990), Chyu and Goldstein (1991), and Jubran et al. (1993) and others have explored various issues such as the differences between short and long pins, the contribution of pin heat transfer versus endwall heat transfer, the presence of an optimal streamwise and spanwise spacing/pitch, etc.

Only recently, with the advent of more powerful computational machines and software tools, have numerical studies of compact heat exchangers been attempted as

reviewed by Shah et al. (2001). For the staggered pin fin array configuration in particular, Donahoo et al. (2001) have used a general purpose viscous flow solver to simulate the fluid flow and heat transfer behavior in a 2-D numerical study. However the 2-D nature cannot be used to treat the endwalls where the pins meet the surface.

The experimental baseline for this study is the Metzger et al. work of 1982. Metzger showed the variation of streamwise heat transfer, overall array heat transfer, and overall flow friction in staggered, short pin fin arrays. His experimental work has provided the baseline for this computer model. His experimental work showed that there was a substantial difference between short pin fin arrays and long cylinder (tube bank) arrays. Long cylinders had been the previous model for the array. The relations Metzger developed for overall heat transfer showed a lower array averaged Nusselt number over the array based on his experiments. The long cylinder predictions did not correctly predict the convection coefficients observed in the short pin fin array.

### **C. OBJECTIVE**

The primary objective of this study was to select a turbulence model that accurately reflects the experimental results seen in previous work. As part of the selection process, the turbulence model had to be optimized since the default coefficients in a model are typically better suited for flat plate or long cylinder tube-bank type open geometries, but not very applicable to confined tortuous flow geometries such as the short pin fin array in this

study. Another objective is to leave the code open for future work where pin shape and spacing/layout could be changed. The goal would be to arrive at a recommendation for the most optimal turbulence model/s and their coefficients that would provide the best corroboration with available experimental data. Furthermore it is hoped that subject to future experimental work, the current findings can be extended to have validity over a wide range of Reynolds numbers and geometrical configurations thus providing greater applicability and confidence in future numerical simulations.

### III. TURBULENCE MODELS

#### A. INITIAL MODELING

##### 1. Boundary Conditions

The numerical model of Metzger's experiment consists of two different boundaries. Fluid elements were defined which had rigid boundaries, eliminating the need for defining a rigid structure to surround the fluid elements. To reduce the number of nodes required for modeling, symmetry was exploited. A horizontal plane, parallel to the flow direction, halfway between the upper and lower isothermal boundaries of the passage defines an adiabatic boundary. No net properties cross this boundary. The length scale in the flow passage is sufficiently small that buoyancy effects are negligible. This boundary was defined as insulated and velocity in the vertical direction was zero. However the no-slip condition along the plane was released. A similar symmetry plane was defined perpendicular to the first symmetry plane and parallel to the flow direction. The boundary was again modeled as insulated, crossing velocity was set to zero and the no-slip condition along the plane was released. These two planes allowed a model to only have nodes in one quadrant as the other quadrants would produce the same result. Observing the downstream direction, the lower-right quadrant was the quadrant chosen for modeling.

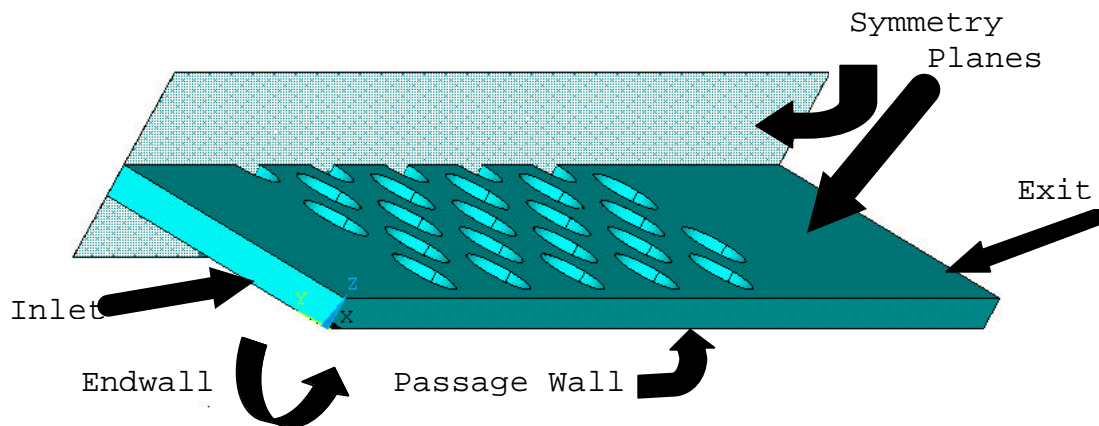


Figure 2. Modeled Portion of a Pin Fin Heat Exchanger

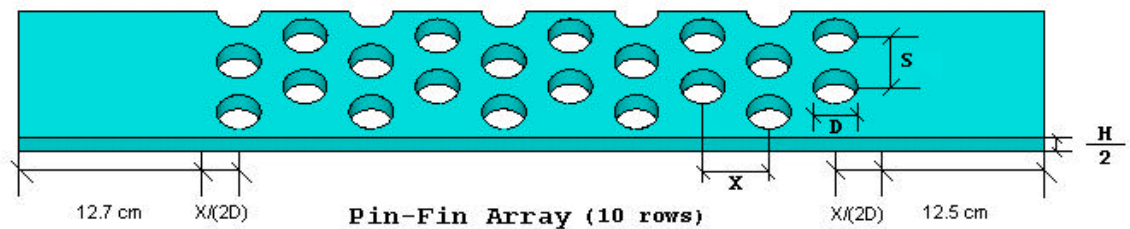


Figure 3. Actual model used for experiment

The pins were modeled as isothermal and so was the supporting endwall. The remaining wall, the sidewall, parallel to the pin axes was insulated. The no slip condition was applied to all boundaries except the symmetry planes. Straight duct entrance and exit regions were attached at the inlet and outlet sections of the array test section to be consistent with the experimental rig of

Metzger et al (1982). They were modeled slightly longer than the Metzger model to prevent the outlet conditions from affecting the test section.

The isothermal boundaries were fixed at 306 K. Dry air (Pr = 0.7) was used as working fluid, entering the inlet section at 300K,  $r=1.1769 \frac{kg}{m^3}$ ,  $m=1.8468 \times 10^{-5} \frac{kg}{m \cdot s}$ ,  $K=2.6294 \times 10^{-2} \frac{W}{m \cdot K}$ , and  $C_p=1004.0 \frac{J}{kg \cdot K}$ . Inlet velocity was specified at the entrance to the test section based on a maximum velocity type Reynolds number.

The maximum velocity Reynolds number is defined as  $Re = \frac{r V_{max} D}{m}$  (Metzger et al., 1982), where  $V_{max}$  is the inviscid, geometry based maximum velocity the fluid reaches when passing through the test section.  $D$  is the pin diameter.

## 2. Initial Conditions

Each run was initiated with the walls and pins of the test section at 306K and the incoming air at 300K. Inlet velocity was determined by the specified Reynolds number and fluid properties.

## 3. Mesh Structure

The mesh was specified to concentrate nodes in the no slip boundary areas of the model, where flow and temperature gradients might be expected to be highest (Fig 4). Around the pins, nodes were concentrated in the high velocity regions where conditions change the most (Fig 5).

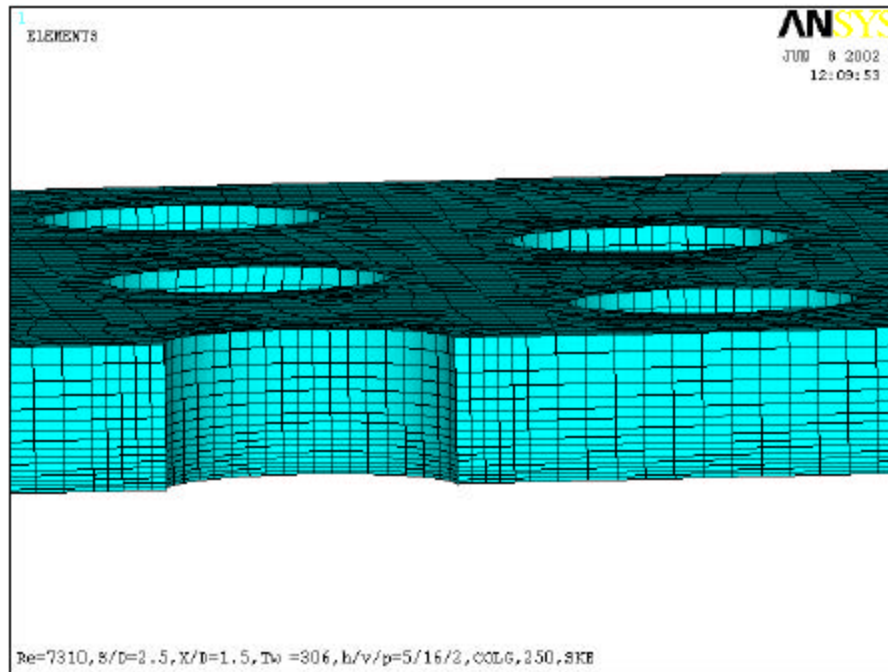


Figure 4. Standard Mesh showing nodes concentrated in the areas of the no slip boundary.

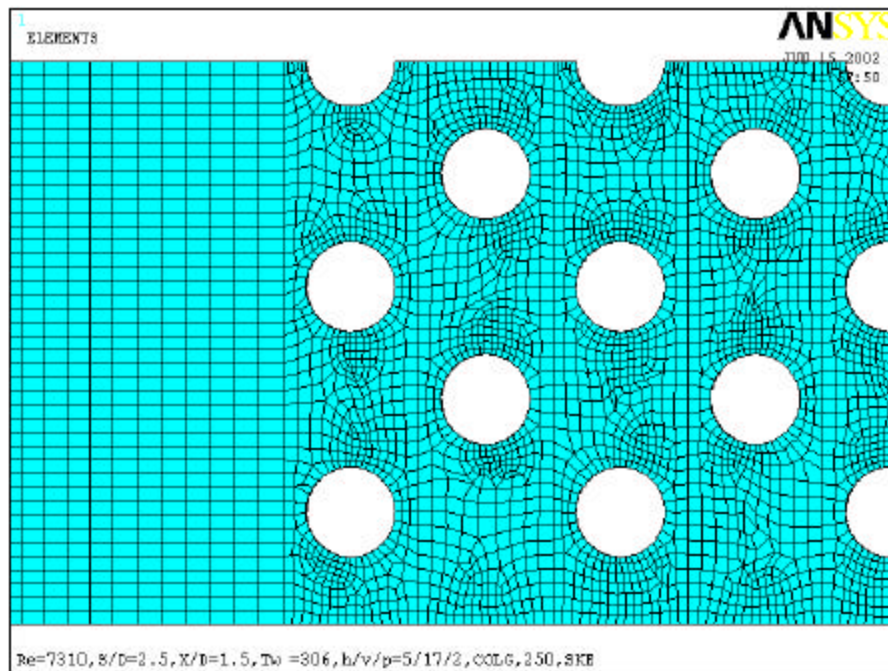


Figure 5. Standard Mesh (Top View) with nodes concentrated around the high velocity regions of the pins

Nodes were also concentrated along the endwall.

For constructing the numerical model of the heat exchanger and for the majority of the data gathering, the finite element based modeling and simulation package, ANSYS was used. The versions available during this research were ANSYS version 5.7, 6.0, and 6.1. The bulk of the research was done using ANSYS 6.0. The ANSYS license at the Naval Postgraduate School (NPS) limited models to 256,000 nodes. Several runs were attempted using the Department of Defense High Performance Computing Major Shared Resource Center (HPCMSRC). The ANSYS license at the HPCMSRC was node unlimited.

At the entrance and exit of the test section, as well as midway between each row of pins (apparent in figures 4 and 5), a vertical plane of nodes was constructed. This allowed bulk temperature and mass flows to be calculated independent of the ANSYS program. Such a layer of nodes would also facilitate future work where pin shape and layout are expected to be changed.

## **B. SKE MODEL**

The Standard k- $\epsilon$  (SKE) Model is the default turbulence model for ANSYS 6.0. The SKE model is a Reynolds Averaged Navier-Stokes (RANS) type of Eddy Viscosity Model (EVM). The SKE model uses 2 equations to close the governing equations. The EVM approach introduces a turbulent viscosity term,  $\mu_t$ , which relates the fluctuating velocities of a turbulent flow to a viscous stress term,

$$-\overline{u_i u_j} = \frac{\mathbf{m}}{\mathbf{r}} \frac{\partial u_i}{\partial x_j}, \text{ in tensor notation, which is used in the}$$

Reynolds stress terms of the time averaged, turbulent, incompressible Navier-Stokes equations, as well as in the energy equation and the continuity equation. As an example, the x component of the Reynolds stress term is:

$$\mathbf{s}_x^R = -\frac{\partial}{\partial x}(\overline{\mathbf{r}V_x'V_x'}) - \frac{\partial}{\partial y}(\overline{\mathbf{r}V_x'V_y'}) - \frac{\partial}{\partial z}(\overline{\mathbf{r}V_x'V_z'}), \text{ where } V_x', V_y', V_z' \text{ are the}$$

fluctuating components of the velocities. The Reynolds stress terms contain the indeterminate part of the Navier-Stokes relations, the mean of the product of the fluctuating velocity components. Replacing that product with the relation involving the turbulent viscosity allows the Navier-Stokes momentum equations, continuity and energy equations to be reshaped. In the SKE model two transport equations are derived from the governing equations, the Turbulent Kinetic Energy equation:

$$\begin{aligned} & \frac{\partial \mathbf{r}k}{\partial t} + \frac{\partial(\mathbf{r}V_x k)}{\partial x} + \frac{\partial(\mathbf{r}V_y k)}{\partial y} + \frac{\partial(\mathbf{r}V_z k)}{\partial z} \\ &= \frac{\partial}{\partial x} \left( \frac{\mathbf{m}}{\mathbf{s}_k} \frac{\partial k}{\partial x} \right) + \frac{\partial}{\partial y} \left( \frac{\mathbf{m}}{\mathbf{s}_k} \frac{\partial k}{\partial y} \right) + \frac{\partial}{\partial z} \left( \frac{\mathbf{m}}{\mathbf{s}_k} \frac{\partial k}{\partial z} \right) + \mathbf{m}_t \Phi \\ & - \mathbf{r}\mathbf{e} + \frac{C_4 \mathbf{b}\mathbf{m}}{\mathbf{s}_t} \left( g_x \frac{\partial T}{\partial x} + g_y \frac{\partial T}{\partial y} + g_z \frac{\partial T}{\partial z} \right) \end{aligned} \quad (1.1)$$

and the Dissipation Rate equation:

$$\begin{aligned} & \frac{\partial \mathbf{r}\mathbf{e}}{\partial t} + \frac{\partial(\mathbf{r}V_x \mathbf{e})}{\partial x} + \frac{\partial(\mathbf{r}V_y \mathbf{e})}{\partial y} + \frac{\partial(\mathbf{r}V_z \mathbf{e})}{\partial z} \\ &= \frac{\partial}{\partial x} \left( \frac{\mathbf{m}}{\mathbf{s}_e} \frac{\partial \mathbf{e}}{\partial x} \right) + \frac{\partial}{\partial y} \left( \frac{\mathbf{m}}{\mathbf{s}_e} \frac{\partial \mathbf{e}}{\partial y} \right) + \frac{\partial}{\partial z} \left( \frac{\mathbf{m}}{\mathbf{s}_e} \frac{\partial \mathbf{e}}{\partial z} \right) + C_{1e} \mathbf{m}_t \frac{\mathbf{e}}{k} \Phi - C_2 \mathbf{r} \frac{\mathbf{e}^2}{k} \end{aligned}$$

$$+\frac{C_m(1-C_3)\mathbf{b}rk}{s_t}\left(g_x\frac{\partial T}{\partial x}+g_y\frac{\partial T}{\partial y}+g_z\frac{\partial T}{\partial z}\right) \quad (1.2)$$

where  $k$  is the turbulent kinetic energy,  $V_x, V_y, V_z$  are the instantaneous (non-fluctuating) velocities,  $s_k$  is the Schmidt number for the transport of turbulent kinetic energy,  $\Phi$  is the viscous dissipation term  $\left(\Phi = \mathbf{m}\left(\frac{\partial u_i}{\partial x_k} + \frac{\partial u_k}{\partial x_i}\right)\frac{\partial u_i}{\partial x_k}\right)$ ,  $e$  is the turbulent kinetic energy dissipation rate,  $C_3$  and  $C_4$  are the buoyancy constants,  $\mathbf{b}$  is the coefficient of thermal expansion,  $s_t$  is the turbulent Prandtl number,  $g$  is the acceleration scalar,  $T$  is the static temperature,  $s_e$  is the Schmidt number for the transport of turbulent kinetic energy dissipation rate,  $C_{le}$  is the shear rate generation term multiplier,  $C_2$  is scaled diffusivity rate multiplier,  $C_m$  is the turbulent viscosity constant, and  $\mathbf{m}$  is the turbulent viscosity broken down in the equation to  $\mathbf{m} = C_m \frac{rk^2}{e}$ . Table 1 contains the values of the SKE constants:

$\mathbf{s}_k$	1.0
$C_3$	1.0
$C_4$	0.0
$\mathbf{b}$	0.0
$\mathbf{s}_t$	1.0
$\mathbf{s}_e$	1.3
$C_{le}$	1.44
$C_2$	1.92
$C_m$	0.09

Table 1. Constants for SKE Model

Solving these equations at each node in the model for a set number of iterations yields values for  $k$  and  $\mathbf{e}$  which are used to calculate  $\mathbf{m}$  from the previous equation.  $\mathbf{m}$  is used to calculate the indeterminate fluctuating velocities in the Navier-Stokes equations. The Navier-Stokes equations are then solved for a new set of mean velocities.

This new set of velocities, with fluctuating components, is then used to solve for temperature in a first law relation:

$$\mathbf{rc} \left( \frac{\partial T}{\partial t} + V_x \frac{\partial T}{\partial x} + V_y \frac{\partial T}{\partial y} + V_z \frac{\partial T}{\partial z} \right) = K \left( \frac{\partial^2 T}{\partial x^2} + \frac{\partial^2 T}{\partial y^2} + \frac{\partial^2 T}{\partial z^2} \right) \quad (1.3)$$

where  $K$  is the thermal conductivity of the fluid, assumed to be isotropic,  $c$  is the specific heat, and the velocities  $V_x, V_y, V_z$  contain the mean and fluctuating components.

The local heat flux,  $q''$ , can be estimated at non-insulated or adiabatic boundaries by the following relation where  $y$  is the direction normal to the transfer surface,

$$q'' = -K \frac{\partial T}{\partial y} \Big|_{y=0}. \quad \text{From this, Newton's Law of Cooling leads to a}$$

convection coefficient,  $h = \frac{q''}{(T_s - T_\infty)}$ , where  $T_s$  is the surface temperature and  $T_\infty$  is the free stream temperature. Since the flow complex, ANSYS 6.0 uses  $T_B$  in place of  $T_\infty$ .  $T_B$  is the bulk temperature of the adjacent fluid element.

The ultimate goal of the simulation is to calculate an array averaged Nusselt number, so an overall array convection coefficient,  $h$ , is calculated based on the total heat transferred to the fluid.

$$h = \frac{q}{A \cdot LMTD} \quad (1.4)$$

where  $q$  is the total amount of heat in watts transferred across the boundaries,  $A$  is the wetted area of the test section, and  $LMTD$  is the Log-Mean Temperature Difference.

$$LMTD = \frac{\Delta T}{\ln \left( \frac{T_{wall} - T_{in}}{T_{wall} - T_{out}} \right)} \quad (1.5)$$

where  $T_{in}$  is the bulk inlet temperature,  $\Delta T$  is calculated from  $\Delta T = \frac{q}{\dot{m} \cdot C_p}$ ,  $T_{wall}$  is the constant isothermal wall temperature for both endwalls and pins, and  $T_{out} = T_{in} + \Delta T$ . The array averaged  $Nu$  is calculated from:

$$Nu = \frac{hD}{K} \quad (1.6)$$

where  $D$  is the diameter of a pin and  $K$  is the thermal conductivity of air evaluated at  $\frac{T_{in} + T_{wall}}{2}$ . This formulation of Nusselt number is the most appropriate for comparing the experimental results of Metzger with the current ANSYS simulations.

One drawback to the SKE model, as well as all the 2 equation EVM's, is that it does not accurately predict turbulent kinetic energy and dissipation rate at elements along the wall. In this case a wall turbulence model is used. The ANSYS default model for wall turbulence is the Van Driest model. The Van Driest model is used at the wall nodes to determine viscosity. It assumes an eddy viscosity of zero at the wall and gives an accurate value for wall conductivity. ANSYS 6.0 uses the continuous Van Driest formulation with the velocity at a certain distance from the wall as a reference velocity. This form of the log law of the wall is solved for a wall viscosity from

$$\frac{V_{tan}}{\sqrt{\frac{t}{r}}} = \frac{1}{k} \left( \ln \frac{E d r}{m_l} \sqrt{\frac{t}{r}} \right) \quad (1.7)$$

where  $\mathbf{t}$  is the shear stress,  $\mathbf{k}$  is the slope of the wall parameter,  $E$  is the Law of the Wall constant,  $\mathbf{m}_l$  is the laminar absolute viscosity, and  $\mathbf{d}$  is the distance from the wall. The wall element effective viscosity,  $\mathbf{m}_w$ , is derived from:

$$\mathbf{m}_w = \mathbf{d} \frac{\mathbf{t}}{V_{\tan}} \quad (1.8).$$

### C. RENORMALIZED GROUP (RNG) MODEL - DIFFERENCES FROM SKE

The RNG model uses an advanced statistical technique called Renormalization Group Theory applied to the instantaneous Navier-Stokes equations. The two transport equations derived for the SKE model appear in the RNG model with the exception of the  $C_{le}$  multiplier for the kinetic energy generation term in the dissipation rate equation. In the RNG model the  $C_{le}$  term takes the form

$$C_{le} = 1.42 - \frac{\mathbf{h} \left( 1 - \frac{\mathbf{h}}{\mathbf{h}_{\infty}} \right)}{1 + \mathbf{b} \mathbf{h}^3} \quad (1.9)$$

where  $\mathbf{h}_{\infty} = 4.38$ ,  $\mathbf{b} = 0.012$ , and  $\mathbf{h}$  is a function of the stress deformation tensor,  $S_{ij}$ . The tensor,  $S_{ij}$ , is a function of velocities in the flowfield,

$$S_{ij} = \frac{1}{2} \left( \frac{\partial V_i}{\partial V_j} + \frac{\partial V_j}{\partial V_i} \right) \quad (1.10).$$

There are differences in the buoyancy terms of the equations but for this heat exchanger as noted earlier buoyancy effects can be ignored. In the RNG model several

constants have different numerical values, the default numerical constants are summarized in Table 2:

$\mathbf{s}_k$	0.72
$C_3$	1.0
$C_4$	0.0
$\mathbf{b}$	0.012
$\mathbf{s}_t$	1.0
$\mathbf{s}_e$	0.72
$\mathbf{h}_\infty$	4.38
$C_2$	1.68
$C_m$	0.085

Table 2. RNG Model Coefficients

This gives the RNG model an added level of complexity and capability over the SKE model due to the more distributed nature of accounting for the turbulent kinetic energy generation term in the flow field. In the SKE model, the kinetic energy generation coefficient in the dissipation rate equation is the same throughout the flowfield. In the RNG model, the coefficient is dependent upon the velocity components at each point in the flow field. ANSYS 6.0 uses a slightly more simplified version than that presented in Numerical Analysis of Compact Heat Exchanger Surfaces (R. K. Shah et al., 2001).

Past research, as noted R. K. Shah et al., describes RNG as being more accurate and reliable than other 2 equation EVM models. Because it is a new model, relatively few studies have been done with it, but it appears to do better than SKE with low Reynolds numbers but worse when vortex shedding becomes an issue, such as with bluff bodies or flow around cylinders as in external flows with open geometries. Although the comparisons were based on 2D models only, RNG's success appears to be highly geometry dependent.

#### D. NKE - DIFFERENCES FROM SKE

The New  $k-\epsilon$  Model (NKE), also known as the Realizable  $k-\epsilon$  Model, was proposed by T. H. Shih et al. in 1994. The model was primarily designed for high Reynolds number flows but has had some success for lower Reynolds number flows as well. The significant differences for a micro heat exchanger type of flow environment are that the NKE model uses a different formulation for the  $C_m$  constant and a different form of the kinetic energy dissipation rate equation.

The turbulent viscosity  $\mu_t$  is still calculated the same way but the  $C_m$  term is now a function of deformation tensors and antisymmetric rotation tensors. ANSYS 6.0 replaces  $C_m$  with this function:

$$C_m = \left( 4 + 1.5 \frac{k}{\epsilon} \sqrt{2 \left( \frac{1}{2} \left( \frac{\partial V_i}{\partial V_j} - V_{j,i} \right)^2 + C_r \Omega_m \epsilon_{mij} \right)^2 + \left( \frac{1}{2} \left( \frac{\partial V_i}{\partial V_j} + V_{j,i} \right) \right)^2} \right)^{-1} \quad (1.11)$$

where the  $C_r \Omega_m \epsilon_{mij}$  term involves the angular velocity of the coordinate system which for this application is not

rotating, so that term drops out. The entire term under the radical is the mean velocity in the law of the wall model.

The dissipation rate equation now becomes:

$$\begin{aligned}
& \frac{\partial \mathbf{r}\mathbf{e}}{\partial t} + \frac{\partial(\mathbf{r}V_x\mathbf{e})}{\partial x} + \frac{\partial(\mathbf{r}V_y\mathbf{e})}{\partial y} + \frac{\partial(\mathbf{r}V_z\mathbf{e})}{\partial z} \\
&= \frac{\partial}{\partial x} \left( \frac{\mathbf{m}_t}{\mathbf{s}_e} \frac{\partial \mathbf{e}}{\partial x} \right) + \frac{\partial}{\partial y} \left( \frac{\mathbf{m}_t}{\mathbf{s}_e} \frac{\partial \mathbf{e}}{\partial y} \right) + \frac{\partial}{\partial z} \left( \frac{\mathbf{m}_t}{\mathbf{s}_e} \frac{\partial \mathbf{e}}{\partial z} \right) + \mathbf{r}C_{le}\mathbf{e} \frac{1}{\sqrt{2}} \sqrt{\left( \frac{\partial V_i}{\partial V_j} + V_{j,i} \right) \left( \frac{\partial V_i}{\partial V_j} + V_{j,i} \right)} \\
& - C_2 \mathbf{r} \frac{\mathbf{e}^2}{k} + \frac{C_m(1-C_3)\mathbf{b}rk}{\mathbf{s}_t} \left( g_x \frac{\partial T}{\partial x} + g_y \frac{\partial T}{\partial y} + g_z \frac{\partial T}{\partial z} \right) \quad (1.12)
\end{aligned}$$

and the  $C_{le}$  multiplier now becomes:

$$C_{le} = \max \left( C_{1M}, \frac{\mathbf{h}}{\mathbf{h}+5} \right) \quad (1.13)$$

where,

$$\mathbf{h} = \frac{k}{2\mathbf{e}} \sqrt{\left( \frac{\partial V_i}{\partial V_j} + \frac{\partial V_j}{\partial V_i} \right) \left( \frac{\partial V_i}{\partial V_j} + \frac{\partial V_j}{\partial V_i} \right)} \quad (1.14)$$

and  $C_{1M}$  is a constant.

The numerical values for the default NKE model are summarized in Table 3:

$\mathbf{s}_k$	1.0
$C_3$	1.0
$C_4$	0.0
$\mathbf{b}$	0.0

$s_t$	1.0
$s_e$	1.2
$C_2$	1.90
$C_{1M}$	0.43

Table 3. NKE Model Coefficients

#### E. FAILURES - ZEM, GIR, SZL

There were three other turbulence models that were evaluated in this study, a zero equation model (ZEM), the non-linear model of Girimaji (GIR), and the Shih, Zhu, Lumley model (SZL). In the Zero Equation Model, the definition of a turbulent viscosity does not introduce another differential equation, and ANSYS calculates a characteristic length applied to the entire model. For this model ANSYS applied a default characteristic length of 1 cm. Neither this characteristic length nor any changes made improved upon the performance of the default SKE model so it was removed from further consideration.

The GIR model was more stable than the ZEM model but it provided results significantly different than the experimental data. It relies on a complex formulation for the  $C_m$  term.

The SZL model is a simpler model than NKE or GIR. It estimates a low level of turbulence for the flowfield and low effective velocity that can quickly become unstable in a complex flowfield. The  $C_m$  term is significantly simpler. It was found that the heat transfer did not steady out

smoothly and it consistently overestimated the parameters used to determine the convection coefficient,  $h$ .

Since each of these 3 models was found wanting compared to the earlier 3, they were not pursued in much further detail in this study.

#### **F. ADVECTION SOLVERS**

For this simulation the ANSYS recommendations for solving complex flow problems were used. Single solvers by themselves did not correctly simulate the flows but combinations of solvers did. For the first 30 iterations the Monotone Streamline Upwind (MSU) advection solver was used for momentum, turbulence, pressure, and temperature. MSU produces first order accurate solutions and is generally very robust. In the current study in particular, after the first 30 iterations, density was permitted to vary and the MSU was still used for momentum, turbulence, pressure, and temperature. For iterations 60 through 90 the momentum was judged stable enough to switch to the Collocated Galerkin (COLG) method, an exact advection solver. For the iterations beyond 90, the COLG solver was used in the solution of momentum, turbulence, pressure, and temperature quantities for best consistency and stability in the final results.

## **IV. RESULTS AND DISCUSSION**

### **A. NUMERICAL EXPERIMENTS CONDUCTED**

In order for a typical numerical run to be considered successful, which could then be compared to other runs with different parameters, a number of numerical performance criteria had to be met. The first and most important was grid independence. To achieve this, the number of elements in the model was increased (in steps of at least 24000 elements) until a less than two percent change was observed in the total heat transfer rate between two consecutive runs. Only one Reynolds number resulted in the heat transferred being outside the 2% limit, and that too was less than 3%.

A second criterion was that no nodal temperature ever went above 306.4K in the last iteration in order to be consistent with the imposed boundary conditions. A third was that the ANSYS generated output bulk temp was within 0.1K of the calculated temperature based on the mass flow rate. The final criterion that had to be met was that the sum of the differences in nodal temperatures between two consecutive iterations divided by the sum of the final nodal temperatures be less than  $1 \times 10^{-4}$  to ensure satisfactory convergence.

Only when all these criteria were met was a run deemed complete, and hence ready for comparison with other completed runs.

### **B. TURBULENCE MODEL PERFORMANCE**

Three models (SKE, RNG, NKE) that were able to meet the above robust benchmark criteria were compared. As

noted earlier, three others (ZEM, GIR, SZL) were also considered initially but failed to meet the basic benchmark criteria and were hence not pursued further.

### **1. The SKE Model**

SKE is the default turbulence model implemented in ANSYS. The model generated stable solutions and in order to compare it with Metzger's experimental work an array averaged Nusselt number was computed for each variation of each model, and compared with its corresponding Metzger setup. Baseline results using SKE as the turbulence model consistently overestimate the Metzger Nusselt number with the exception of the high Reynolds number run in the tightest ( $X/D=1.5$ ) configuration considered. Various coefficients in the SKE turbulent kinetic energy and dissipation rate equations (1.1-.2) could be varied. Four out of a possible nine coefficients were chosen as the ones effecting the most critical changes while the others either dealt with buoyancy terms or were already accounted for by varying the chosen four. Each parameter was varied by an arbitrarily chosen value of 30% up and/or down from its default value and a run was made with only that parameter changed, i.e. all else was held fixed. After every run benchmarks were checked and a comparison with Metzger's Nusselt number was made. Table 4 summarizes SKE performance with respect to changes in  $C_{1e}$ .

Reynolds Number	X/D	S/D	Variable Changed	Percent Changed	Simulated Nu	Experimental Nu	Percent Difference
3980	1.5	2.5	Default	0	33.84	32.28	4.83
3980	1.5	2.5	C1-epsilon	+30	32.19	32.28	-0.28
3980	1.5	2.5	C1-epsilon	-30	39.83	32.28	23.39
7310	1.5	2.5	Default	0	50.58	49.61	1.96
7310	1.5	2.5	C1-epsilon	+30	50.67	49.61	2.14
7310	1.5	2.5	C1-epsilon	-30	57.66	49.61	16.23
13800	1.5	2.5	Default	0	71.71	77.75	-7.77
13800	1.5	2.5	C1-epsilon	+30	74.11	77.75	-4.68
13800	1.5	2.5	C1-epsilon	-30	78.35	77.75	0.77
3590	2.5	2.5	Default	0	29.92	26.73	11.93
3590	2.5	2.5	C1-epsilon	+30	24.58	26.73	-8.04
3590	2.5	2.5	C1-epsilon	-30	36.13	26.73	35.17
7340	2.5	2.5	Default	0	45.69	44.99	1.56
7340	2.5	2.5	C1-epsilon	+30	40.02	44.99	-11.05
7340	2.5	2.5	C1-epsilon	-30	52.65	44.99	17.03
13900	2.5	2.5	Default	0	70.60	71.61	-1.41
13900	2.5	2.5	C1-epsilon	+30	61.65	71.61	-13.91
13900	2.5	2.5	C1-epsilon	-30	76.49	71.61	6.81

Table 4. Summary of SKE performance when  $C_{1e}$  is varied

The  $C_{1e}$  constant precedes the viscous dissipation term in the dissipation rate equation (1.2). Increasing the coefficient generally results in a lower approximation of the Nusselt number than the default case. Specifically the increase in  $C_{1e}$  contributes to an increase in the source term of the dissipation rate transport equation and results in a decrease in the turbulent kinetic energy. The case of Reynolds number of 13800 does not follow the same trend as the other Reynolds numbers. Figure 6 shows this decrease in turbulent kinetic energy as displayed by ANSYS 6.0, the view is from the adiabatic plane looking down towards the lower isothermal plane. The top figure is the default case

and the lower figure is with the increased  $C_{le}$  multiplier  
(note the scale of the colors).

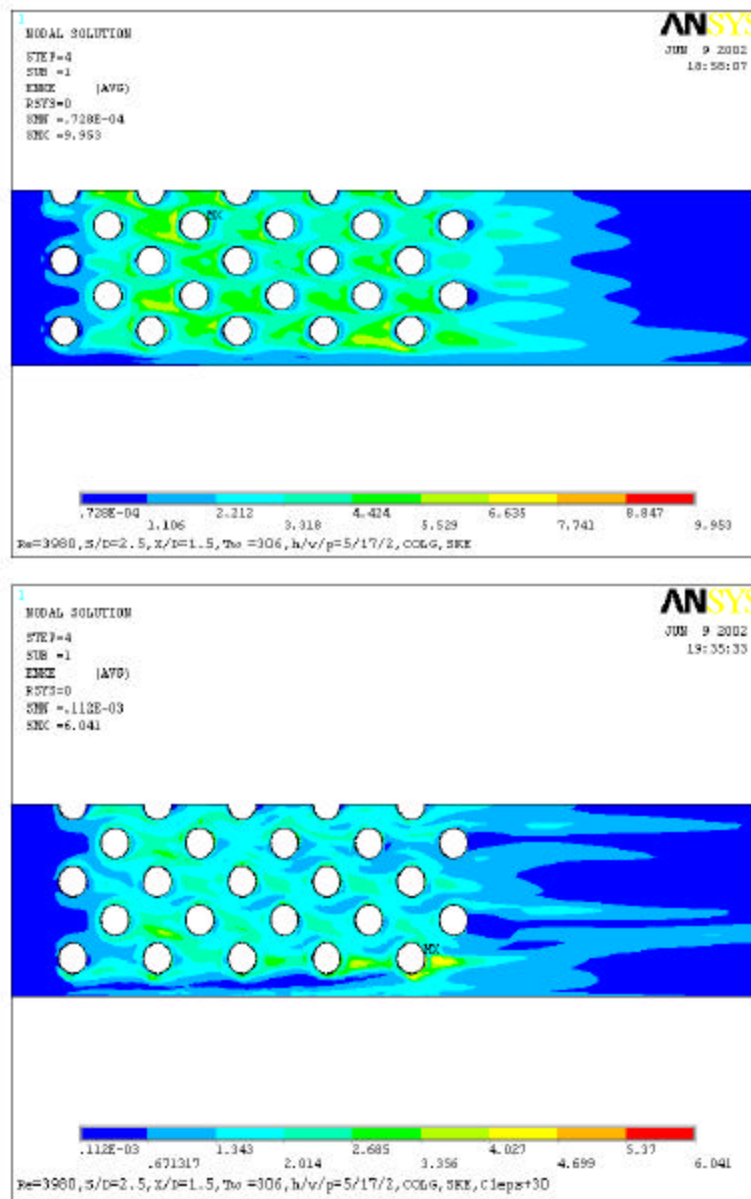


Figure 6. Changes in the turbulent kinetic energy  
in the simulated flow field due to a  $C_{le}$  increase  
of 30% at  $Re=3980$

In exploring the role of the  $C_2$  coefficient, it must be noted that  $C_2$  also contributes to the source term of the dissipation rate transport equation (1.2) in a nonlinear manner and it was found that a decrease in  $C_2$  leads to a decrease in turbulent kinetic energy at each node. The trend seen in Table 5 shows that decreasing  $C_2$  leads to lower Nusselt numbers than in the default SKE case, again with the exception of the case of  $Re = 13800$ . The effect of  $C_2$  on the model increases at higher Reynolds numbers.

Decreasing the turbulent Schmidt number for the transport of dissipation rate,  $s_e$ , affects only the diffusive terms of the dissipation rate transport equation (1.2). A decrease in  $s_e$  leads to an increase in the effective diffusivity of the dissipation rate. Table 5 shows that a change in  $s_e$  has very little impact on the default SKE Nusselt number. The model at  $Re=13900$  was run on a different mesh than the default SKE model therefore no conclusions can be drawn from the large difference.

The turbulent Schmidt number for the transport of kinetic energy,  $s_k$ , is the only parameter that affects the turbulent kinetic energy transport equation (1.1) through the diffusive terms. A decrease in  $s_k$  increases the effective diffusivity of the turbulent kinetic energy. Table 5 shows that the decrease in  $s_k$  has a very small effect on the default Nusselt number similar to the small effect of  $s_e$ .

Reynolds Number	X/D	S/D	Variable Changed	Percent Changed	Simulated Nu	Experimental Nu	Percent Difference
3980	1.5	2.5	Default	0	33.84	32.28	4.83
3980	1.5	2.5	C2	-30	32.90	32.28	1.92
3980	1.5	2.5	Sigma-E	-30	33.86	32.28	4.89
3980	1.5	2.5	Sigma-K	-30	34.32	32.28	6.32
7310	1.5	2.5	Default	0	50.58	49.61	1.96
7310	1.5	2.5	C2	-30	49.83	49.61	0.44
7310	1.5	2.5	Sigma-E	-30	49.82	49.61	0.42
7310	1.5	2.5	Sigma-K	-30	49.95	49.61	0.69
13800	1.5	2.5	Default	0	71.71	77.75	-7.77
13800	1.5	2.5	C2	-30	73.59	77.75	-5.35
13800	1.5	2.5	Sigma-E	-30	71.29	77.75	-8.31
13800	1.5	2.5	Sigma-K	-30	71.17	77.75	-8.46
3590	2.5	2.5	Default	0	29.92	26.73	11.93
3590	2.5	2.5	C2	-30	23.89	26.73	-10.62
3590	2.5	2.5	Sigma-E	-30	29.06	26.73	8.72
3590	2.5	2.5	Sigma-K	-30	29.39	26.73	9.95
7340	2.5	2.5	Default	0	45.69	44.99	1.56
7340	2.5	2.5	C2	-30	40.00	44.99	-11.09
7340	2.5	2.5	Sigma-E	-30	44.88	44.99	-0.24
7340	2.5	2.5	Sigma-K	-30	44.88	44.99	-0.24
13900	2.5	2.5	Default	0	70.60	71.61	-1.41
13900	2.5	2.5	C2	-30	56.06	71.61	-21.71
13900	2.5	2.5	Sigma-E	-30	60.89	71.61	-14.97
13900	2.5	2.5	Sigma-K	-30	60.44	71.61	-15.60

Table 5. Summary of SKE performance when  $C_2$ ,  $s_e$ , and  $s_k$  are decreased by 30%

For the SKE model, general trends observed were that for the lower Reynolds numbers (3980, 7310, 3590, 7340) the default SKE model overestimated the Nusselt number for the array. For higher Reynolds numbers (13800, 13900) the trend was reversed and the default SKE model consistently underestimated the experimental Nusselt number. This trend seems to be independent of the longitudinal spacing (X) between pins.

## 2. The RNG Model

The next model analyzed was the RNG model. For each Reynolds number a run was carried out for the default model settings. The resulting Nu was compared to the same

experimental Nu from the SKE runs. There are 10 model coefficients in the RNG model that can be modified using ANSYS 6.0. Only two of these parameters ( $h_{\infty}$  and  $b$ ) have a different effect on the two transport equations (1.1-2) compared to the SKE model. Both of these parameters are the multipliers in the RNG formulation for  $C_{le}$ , equation (1.9). The constant  $h_{\infty}$  has the greatest effect of the two on the  $C_{le}$  formulation. Hence this was selected as the only parameter to vary in the RNG trials; the others were unchanged from the SKE model since they had been accounted for in those trial runs. The value of  $h_{\infty}$  in the RNG model was also changed by 30% up and down from its default setting. Table 6 summarizes the resulting changes.

Reynolds Number	X/D	S/D	Variable Changed	Percent Changed	Simulated Nu	Experimental Nu	Percent Difference
3980	1.5	2.5	Default	0	33.55	32.28	3.93
3980	1.5	2.5	Eta-inf	+30	36.80	32.28	14.00
3980	1.5	2.5	Eta-inf	-30	33.82	32.28	4.77
7310	1.5	2.5	Default	0	49.40	49.61	-0.42
7310	1.5	2.5	Eta-inf	+30	52.51	49.61	5.85
7310	1.5	2.5	Eta-inf	-30	50.88	49.61	2.56
13800	1.5	2.5	Default	0	71.00	77.75	-8.68
13800	1.5	2.5	Eta-inf	+30	73.33	77.75	-5.68
13800	1.5	2.5	Eta-inf	-30	75.13	77.75	-3.37
3590	2.5	2.5	Default	0	29.00	26.73	8.49
3590	2.5	2.5	Eta-inf	+30	32.63	26.73	22.07
3590	2.5	2.5	Eta-inf	-30	25.36	26.73	-5.13
7340	2.5	2.5	Default	0	44.25	44.99	-1.64
7340	2.5	2.5	Eta-inf	+30	48.45	44.99	7.69
7340	2.5	2.5	Eta-inf	-30	40.19	44.99	-10.67
13900	2.5	2.5	Default	0	68.32	71.61	-4.59
13900	2.5	2.5	Eta-inf	+30	72.58	71.61	1.35
13900	2.5	2.5	Eta-inf	-30	62.83	71.61	-12.26

Table 6. Summary of RNG Performance When  $h_{\infty}$  is Varied

The RNG results for the default model underestimate the experimental Nusselt for all but the lowest 2 Reynolds numbers. This trend is independent of the  $X/D$  ratio. For the lowest Reynolds numbers the RNG default model overestimates the Nusselt number. The RNG is a more sophisticated model in that it takes into account the variation of the turbulent kinetic energy in the flow field when determining the  $C_{le}$  term. However this added parameter provides a more accurate Nusselt number than the SKE model only at Reynolds numbers less than or equal to 7340. This agrees with prior work described by Shah et al (2001) for 2-D cases using the RNG model in similar flow scenarios. Varying the constant  $h_{\infty}$  does not have predictable results. Increasing the constant by 30% always pushes the simulated Nusselt number higher. Decreasing the constant has less predictable results, but in the extended configuration ( $X/D = 2.5$ ), decreasing  $h_{\infty}$  decreased the Nusselt number. This appears to be geometry dependent. The results of decreasing  $h_{\infty}$  can be seen in the change of the distribution of turbulent kinetic energy in the flow field for the 3980 Reynolds number in Figure 7. Figure 8 shows the difference in the temperature field for the same conditions. Both views are looking down through the adiabatic plane.

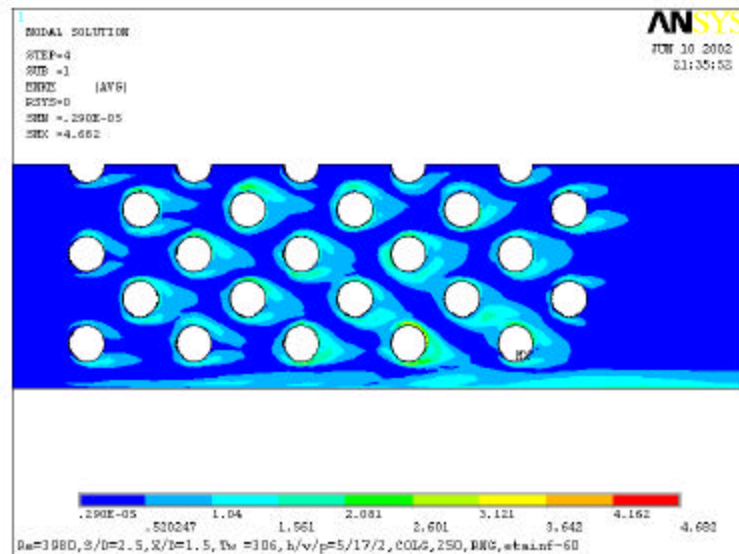
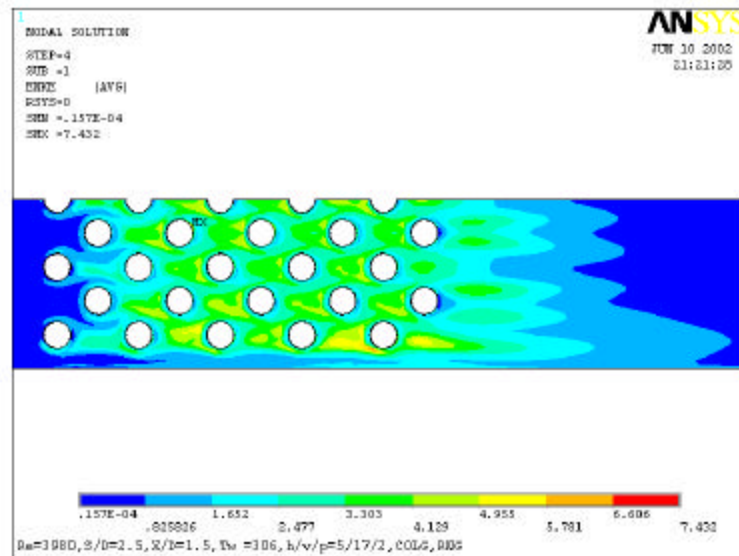


Figure 7. Change in the turbulent kinetic energy distribution of an RNG run at  $Re=3980$  where  $h_{\infty}$  was decreased by 60%

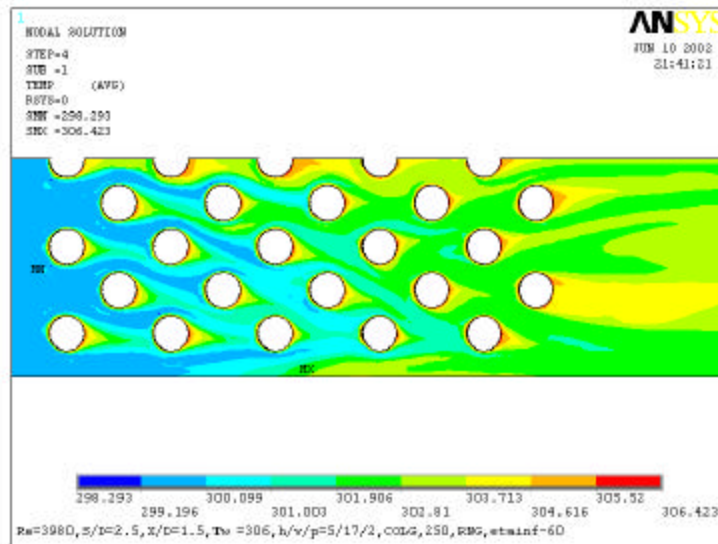
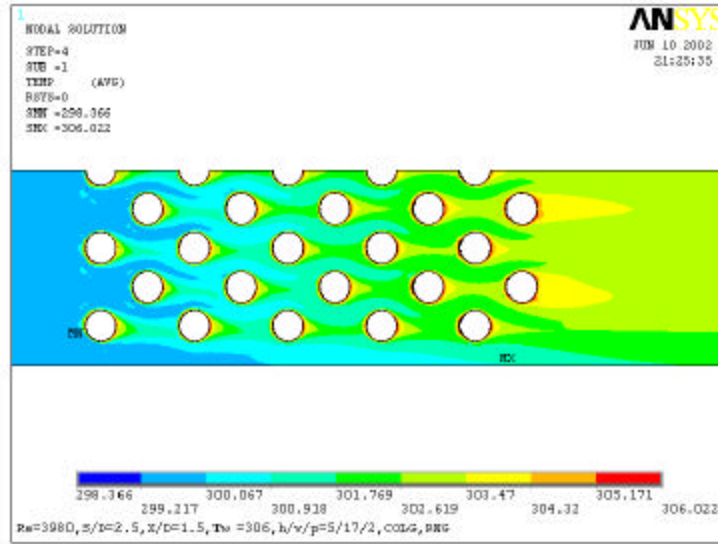


Figure 8. Change in the temperature distribution of an RNG run at  $Re=3980$  where  $h_{\infty}$  was decreased by 60%

In other runs it was observed that any change up or down in the  $C_2$  constant brought a change in the Nusselt number in the same direction. The constant  $C_2$  was a consistent predictor but its effectiveness decreased the greater the change in the constant. It was unable to change the Nusselt numbers by enough to bring them closer

to the experimental values without causing the transport equations to become unstable.

Other runs also included runs where  $C_m$  was decreased by 30%. The Nusselt number changed in the same direction for all Reynolds numbers for a given spacing configuration. When  $X/D=1.5$ , decreases in  $C_m$  brought increases in the Nusselt number with respect to the default RNG runs. However when  $X/D=2.5$ , decreases in  $C_m$  resulted in decreases in the Nusselt number.

### **3. The NKE Model**

The next model run was the New  $k-\epsilon$  (NKE) Model. This model is proposed in the literature as being suitable for high Reynolds numbers. The model bears this out for its default case. The difference between the simulated and experimental Nusselt numbers decreases as Reynolds number increases but only for the cases of  $X/D=1.5$ . At  $Re=13900$  the numerical runs were unsuccessful. The results are summarized in Table 7. The values of  $C_{IM}$  were chosen to be evenly spaced between 0.43 and 1.0. The lower number, 0.43, corresponds with the default setting, and 1.0 corresponds with the limit of  $\frac{h}{h+5}$  as  $h$  goes to infinity.

Reynolds Number	X/D	S/D	Variable Changed	Value	Simulated Nu	Experimental Nu	Percent Diff.
3980	1.5	2.5	Default	0.43	35.94	32.28	11.34
3980	1.5	2.5	C1M	0.6	31.44	32.28	-2.60
3980	1.5	2.5	C1M	0.8	32.88	32.28	1.86
7310	1.5	2.5	Default	0.43	53.53	49.61	7.90
7310	1.5	2.5	C1M	0.6	46.91	49.61	-5.44
7310	1.5	2.5	C1M	0.8	50.71	49.61	2.22
13800	1.5	2.5	Default	0.43	74.87	77.75	-3.70
13800	1.5	2.5	C1M	0.6	70.23	77.75	-9.67
13800	1.5	2.5	C1M	0.8	75.97	77.75	-2.29
3590	2.5	2.5	Default	0.43	31.66	26.73	18.44
3590	2.5	2.5	C1M	0.6	25.17	26.73	-5.84
3590	2.5	2.5	C1M	0.8	25.00	26.73	-6.47
7340	2.5	2.5	Default	0.43	46.45	44.99	3.25
7340	2.5	2.5	C1M	0.6	38.67	44.99	-14.05
7340	2.5	2.5	C1M	0.8	39.07	44.99	-13.16
13900	2.5	2.5	Default	0.43	-	71.61	
13900	2.5	2.5	C1M	0.6	-	71.61	
13900	2.5	2.5	C1M	0.8	-	71.61	

Table 7. Summary of NKE Performance

Changing the  $C_{IM}$  constant for the X/D case of 1.5 results in improved performance between 0.6 and 0.8, increasing to 0.8 for the highest Reynolds number of the X/D = 1.5 case. In the X/D = 2.5 case changing the  $C_{IM}$  constant has a mixed effect.

## V. CONCLUSIONS AND RECOMENDATIONS

### A. OPTIMIZATION OF THE SHORT PIN FIN HEAT EXCHANGER

Table 8 shows the optimal constants for the short pin fin heat exchanger. There is substantial improvement in the  $X/D=1.5$  spacing ratio model. The lower Reynolds number flows, regardless of spacing ratio, are not well represented by the SKE default model. The SKE default model consistently overestimates the amount of turbulent kinetic energy in low Reynolds number flows resulting in simulated flows with high Nusselt numbers. The increase in the  $C_{le}$  constant and the reduction in the  $C_m$  constant weight terms in their specific models to decrease turbulent kinetic energy and increase the dissipation rate. This can also be seen in Table 4 where  $C_{le}$  is increased by 30% and this drives the dissipation rate up as the transport equations (1.1-.2) are solved resulting in a lower Nusselt number, closer to the experimental value.

Reynolds	Model	Variable Combination	Simulated Nu	Experimental Nu	SKE Def. Nu	Percent Improvement
3980	SKE	C1+30	32.19	32.28	34.81	96.44
7310	RNG	Default	49.40	49.61	50.58	78.35
13800	SKE	C1-30	78.35	77.75	71.71	90.07
3590	RNG	Cmu-30	26.37	26.73	29.92	88.71
7340	SKE	Default	45.69	44.99	45.69	0.00
13900	RNG	Eta+30	72.58	71.61	70.60	3.96

Table 8. Optimal Constants for the Cross Flow Pin Fin Heat Exchanger.

Table 9 shows the performance of the optimal constants against Metzger's values.

Reynolds Number	Model	Variable Combination	Simulated Nu	Experimental Nu	Percent Difference
3980	SKE	C1+30	32.19	32.28	-0.28
7310	RNG	Default	49.40	49.61	-0.42
13800	SKE	C1-30	78.35	77.75	0.77
3590	RNG	Cmu-30	26.37	26.73	-1.35
7340	SKE	Default	45.69	44.99	1.56
13900	RNG	Eta+30	72.58	71.61	1.35

Table 9. Optimal Constants Compared with Metzger's Experimental Values

## B. FUTURE PLANS

The next steps for this study should be to explore changes to terms in the models that affect the balance of turbulent kinetic energy and the turbulent kinetic energy dissipation rate (1.1-.2). This balance seems to have the most significant effect on the performance of a turbulence model. Specific changes need to be in exploring a reduction of the  $C_{le}$  constant for higher Reynolds numbers in the expanded configuration ( $X/D=2.5$ ) of the SKE model. There is a possibility that the viscous dissipation term becomes greater as the flow moves farther downstream and away from turbulence creating obstructions such as the pins. Table 4 shows that the changes of +/- 30% of  $C_{le}$  bracket the experimental Nusselt number with the exception of the  $Re=7310$  run. This leads to varying constants in the model that are directly tied to source and dissipation terms as  $C_{le}$  is. Iterating the percent change should bring that constant into close agreement with the experimental value. Another specific area is the higher Reynolds number

performance of the RNG model. The  $h_{\infty}$  constant does not provide predictable improvements for the model. At higher Reynolds numbers there may be a benefit in increasing the  $C_2$  term that reduces the contribution of the viscous dissipation rate, which appears as  $e^2$ .

For future considerations, temperature differences must be increased to more accurately model environmental temperatures, H/D ratios should be varied slightly (0.5-2.0) to see where these relations need to be improved.

Another environmental concern is to model the rotational environment experienced in a gas turbine's power turbine. For further heat transfer performance refinement, attention will have to be paid to the variations available for the wall turbulence model.

Many compact heat exchangers use different pin shapes than cylinders. The ANSYS code has been written with vertical planes midway between each row that will facilitate changing entire rows to different span wise spacing and pin shapes.

THIS PAGE INTENTIONALLY LEFT BLANK

## LIST OF REFERENCES

- ANSYS Inc., *ANSYS Theory Reference*, ANSYS Inc., 2001.
- Chyu, M.K., "Heat Transfer and Pressure Drop for Short Pin-Fin Arrays with Pin-Endwall Fillet", *Journal of Heat Transfer*, Vol. 112, pp. 926-932, 1990.
- Chyu, M.K., and Goldstein, R.J., "Influence of Cylindrical Elements on Local Mass Transfer From a Flat Surface", *Int. J. Heat Mass Transfer*, Vol. 34, pp. 2175-2186, 1991.
- Donahoo, E.E., Camci, C., Kulkarni, A.K., Belegundu, A.D., "Determination of Optimal Row Spacing for a Staggered Cross-Pin Array in a Turbine Blade Cooling Passage", *Enhanced Heat Transfer*, Vol. 8, pp. 41-53, 2001.
- Incropera, F. P., Dewitt, D. P., *Introduction to Heat Transfer*, 3rd ed., John Wiley and Sons, 1996.
- Jubran, B. A., Hamdan, M.A., Abdualh, R.M., "Enhanced Heat Transfer, Missing Pin, and Optimization for Cylindrical Pin Fin Arrays", *ASME Journal of Heat Transfer*, Vol. 115, pp. 576-583, 1993.
- Kays, W. M., Crawford, M. E., *Convective Heat and Mass Transfer*, 3<sup>rd</sup> ed., McGraw-Hill, Inc., 1993.
- Metzger, D. E., Berry, R. A., Bronson, J. P., "Developing Heat Transfer in Rectangular Ducts With Staggered Arrays of Short Pin Fins", *Journal of Heat Transfer*, Vol. 104, pp. 700-706, 1982.
- Shih, TH., Zhu, J., Lumley, J. L., "A New Reynolds Stress Algebraic Equation Model", *Computer Methods in Applied Mechanics and Engineering*, Vol. 125, pp. 287-302, 1995.
- Shah, R. K., Heikal, M. R., Thonon, B., Tochon, P., "Progress in the Numerical Analysis of Compact Heat Exchanger Surfaces", *Advances in Heat Transfer*, Vol. 34, pp. 363-443, 2001.

VanFossen, G. J., "Heat-Transfer Coefficients for Staggered Arrays of Short Pin Fins", Journal of Engineering for Power, Vol.104, pp. 268-274, 1982.

White, F. M., *Fluid Mechanics*, 4th ed., WCB/McGraw-Hill, 1999.

White, F. M., *Viscous Fluid Flow*, 1st ed., McGraw-Hill, Inc., 1974.

## INITIAL DISTRIBUTION LIST

1. Defense Technical Information Center  
Ft. Belvoir, VA
2. Dudley Knox Library  
Naval Postgraduate School  
Monterey, CA
3. Terry McNelley, Chairman, Code ME  
Naval Postgraduate School  
Monterey, CA
4. Professor Ashok Gopinath, Code ME/Gk  
Department of Mechanical Engineering  
Naval Postgraduate School  
Monterey, CA
5. Naval/Mechanical Engineering Curricular Office  
Code 34  
Naval Postgraduate School  
Monterey, CA
6. Eric K. Lind  
Pacific Grove, CA